Original

Su, J.; Pohlmann, T.:

Wind and topography influence on an upwelling system at the eastern Hainan coast

In: Journal of Geophysical Research (2009) AGU

DOI: 10.1029/2008JC005018

Wind and topography influence on an upwelling system at the eastern Hainan coast

Jian Su[1,2] and Thomas Pohlmann[1]

Received 13 July 2008; revised 27 January 2009; accepted 24 March 2009; published 19 June 2009.

[1] During the summer monsoon, an upwelling dominates east of Hainan Island, which can be observed by means of field studies and satellite sea surface temperature images. The centers of cold water at the surface always show a strong patchiness. A 3-D high-resolution model is applied to study the impact of the topography on the wind-driven upwelling system. The experiments show that the upwelling-favoring wind is the main driving force, and we concluded that the formation of the centers of cold water at the surface significantly depends on the strength of southwesterly and southerly winds. Moreover, the internal waves are generated at the shelf break representing the most prominent interaction between inner shelf and open ocean. The alongshore topographic variations play an important role in the distribution of the upwelling centers. This combined effect of wind and topography leads to the following processes: (1) When the southwesterly or southerly wind is strong enough, topographic variations cause upwelling centers at the downstream side of topographic high and a downwelling center at the upstream side which in turn lead to density variations. (2) These density variations cause additional pressure gradients which advect the upwelling centers toward the northeast. (3) A longer period of upwelling favorable winds support the advection processes which cause an enlargement of the cold water centers. All these processes together can explain the observed uneven distribution of upwelling centers.

Citation: Su, J., and T. Pohlmann (2009), Wind and topography influence on an upwelling system at the eastern Hainan coast, *J. Geophys. Res.*, *114*, C06017, doi:10.1029/2008JC005018.

1. Introduction

[2] Upwelling along the northern South China Sea (SCS) coast was reported by *Shaw and Chao* [1994] and also observed at the west coast of the SCS by satellite observations [*Kuo*, 2000; *Chu et al.*, 1999; *Xie et al.*, 2003]. In summer, under the southwesterly monsoon forcing, a northeastward current flows along the Vietnam coast, the south and east coast of Hainan Island, and the northern SCS coast. This strong current is denoted as a western boundary current occuring in the SCS [*Su*, 2004], *Chu et al.* [1999] calculated the transport volume of this current to be 5.5 Sv. In this study, we focus on the east coast of Hainan Island which is in the main path of this strong current when it moves offshore toward the Vietnamese coast. Wind induced upwelling according to *Ekman* [1905] is the main process under investigation in most publications. However, there are some theoretical studies showing the importance of topography in the wind-driven upwelling system [*Song et al.*, 2001; *Song and Chao*, 2004]. The theoretical model results indicate that topographic variations do not change the total amount of upwelled water but redistribute it unevenly along the coast to form enhanced upwelling. *Rosenfeld et al.* [1994] proposed a conceptual model to explain the upwelling at capes in Monterey Bay. They showed that Ekman transports around capes cause an alongshore pressure gradient which force a bifurcation of the flow field. *Oke and Middleton* [2000] demonstrated through numerical simulations that topographic acceleration of the East Australian Current (EAC) plays a role in driving upwelling.

[3] Hainan Island is the largest island in the SCS and is located in the northwest of the SCS (Figure 1). Coastal upwelling has attained attention from researchers mainly concerning the northern SCS, but there are few studies concerning the Hainan area [*Hu et al.*, 2003]. Upwelling near Hainan Island is concentrated at the east of the island, between 18°30′–20°30′N and 110°–111°30′E, which relates to the general circulation in the SCS [*Deng and Zhong*, 1995]. Using available observations, *Guo et al.* [1998] used a two dimensional diagnostic model calculating the maximum vertical velocity to be 3.21×10^{-5} m s^{-1}, located in 30 m water depth and 10 km offshore. *Chai et al.* [2001] studied the dynamics and interannual variability of upwelling and how it relates to the ecosystem east of Hainan Island. However, there are still many questions remaining, on the basis of the previous studies, like what is the mechanism controlling the structure of patchiness and what is the role of topographic effects? Therefore, a modeling study to better understande the mechanisms controlling the upwell-

[1]Institute of Oceanography, Centre for Marine and Climate Research, University of Hamburg, Hamburg, Germany.
[2]Institute for Coastal Research, GKSS Research Center, Geesthacht, Germany.

0148-0227/09/2008JC005018

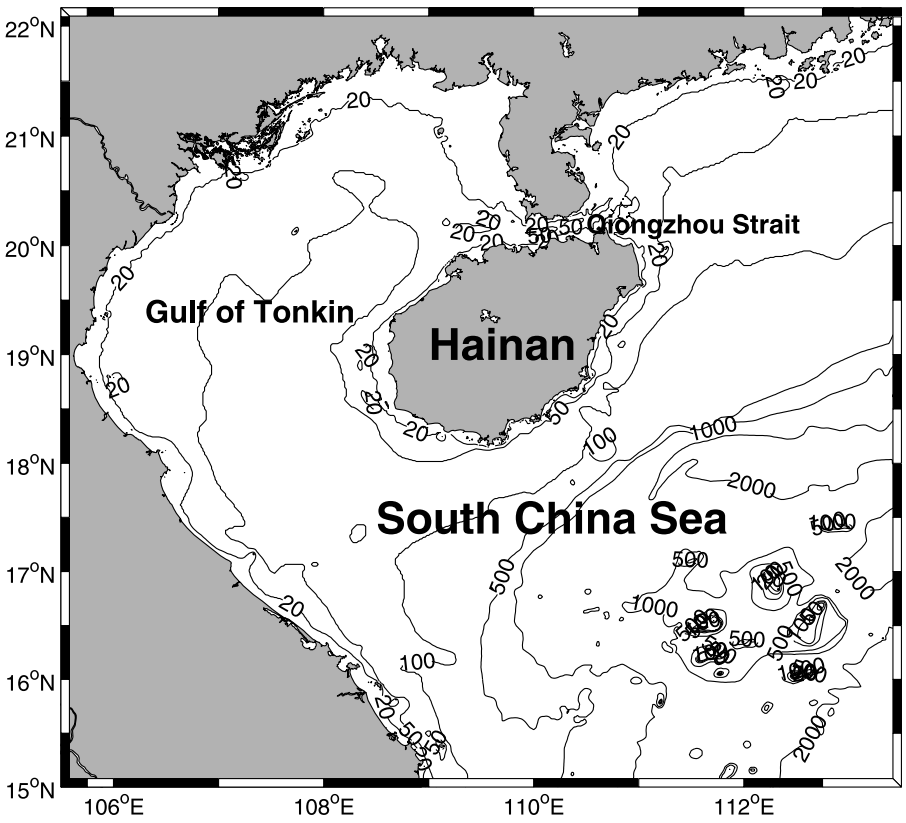

Figure 1. Topography (m) of the model area, which is located in the northwestern South China Sea. The area of interest is east of Hainan Island where upwelling occurs in summer.

ing is necessary. In particular, we try to determine the role of topography in the formation of upwelling east of the Hainan Island.

[4] When there are persistent upwelling-favorable winds during the summer monsoon, Ekman upwelling is the dominant feature east of the Hainan Island. However, in this typical boundary current system, alongshore topographic variation can also play an important role. *MacCready and Rhines* [1993] build a bottom boundary layer (BBL) shutdown process theory using the geostrophic assumption and the thermal wind relation. They applied this theory to the EAC system and were able to show the importance of the topographic variation for the upwelling. Even though, this BBL shut down process was not prevailing, the study in the EAC system demonstrated that enhanced vertical mixing induced by alongshore topographic variation is the dominant factor for the dynamics on this upwelling system [*Oke and Middleton*, 2000]. In the north of Hainan, Qiongzhou Strait, a narrow shallow strait with a sill depth of 20 m separates the island from the mainland. The depth of the entire area is less than 100 m. The southeastern coastal zone of Hainan, where upwelling prevails, exhibits a very narrow continental shelf of approximately 100 km width followed by a steep continental slope (Figure 1). Basically, the east coast of Hainan Island runs parallel to the continental slope, whereas in the southern and northern parts the shelf is wider. There are four capes along the coast, Chin-mu Chiao, Ling-shui Chiao, Ta-hua Chiao and Tung-ku Chiao from south to north. To facilitate in the description of different areas, we number the areas centered around these capes as area 1 to 4 (Figure 2). Area 3 located in north of Ta-hua Chiao includes several bays. Obviously, the bottom topography in the east of Hainan Island is extremely complex (Figure 2), what may have a great influence on the hydrographic processes. One of the main achievements of the paper is that it provides information about the dominant dynamics in each of these areas.

[5] *Yang and Price* [2000] did some idealized experiments to prove the impact of the topographic variation on the circulation in the basin. They derived the simplified PV integral constraint

$$\sum_{i=1}^{N} \frac{Q_i f_i}{H_i} = -\lambda \oint_C (\mathbf{u}_h \mathbf{l}) dx, \tag{1}$$

where Q_i is volume transport at the ith opening of the basin, f is the Coriolis parameter, λ is the Rayleigh friction coefficient, $\mathbf{u}_h = (u, v)$ is the horizontal velocity vector and $\mathbf{l}$ is unit vector tangential to the lateral boundary. If we assume a flow over a sill, with a sill depth of H_C, and a thickness of the interior ocean of H_I, then equation (1) changes to

$$Qf\left(\frac{1}{H_C} - \frac{1}{H_I}\right) = -\lambda \oint_C (\mathbf{u}_h \mathbf{l}) ds, \tag{2}$$

obviously $H_C < H_I$, therefore, the PV source is positive, and the net friction torque must be positive to achieve the PV balance. This indicates an anticyclonic circulation flow

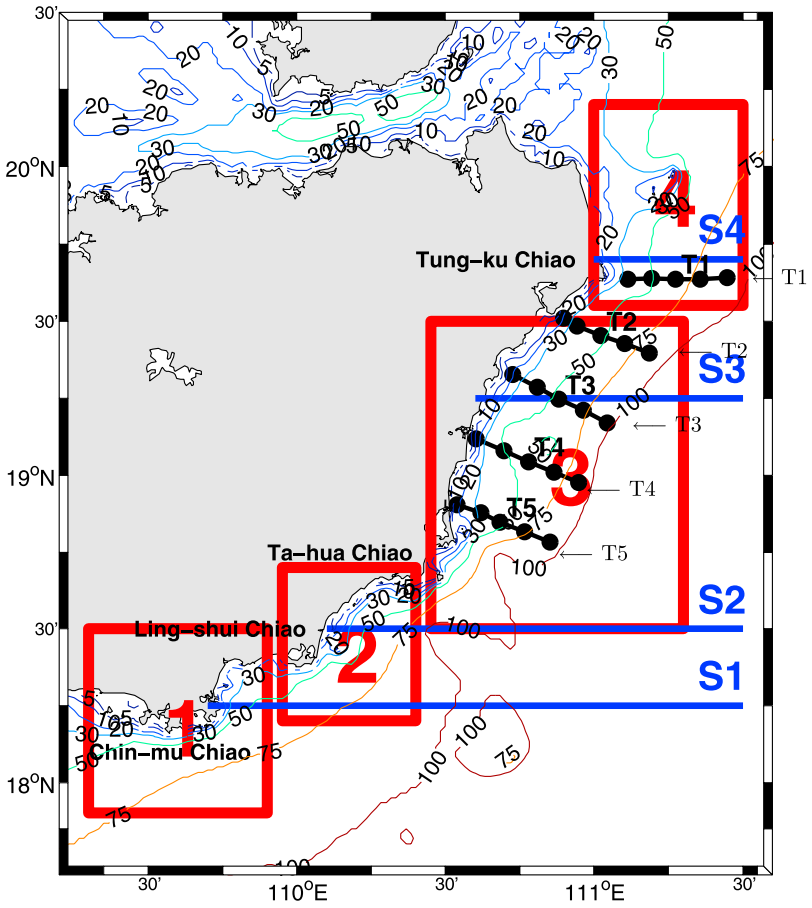

Figure 2. Detailed topography (m) with sampling sites in the east of Hainan Island, five sections T1–T5 from north to south. The black dots are sampling stations. Red squares indicate the different subareas which are numbered by 1–4 from south to north. Area 1–3 represent three bays and area 4 is a cape. The blue lines (S1–S4) show the location of model cross sections.

along the basin boundary when a current approaches a cape on the northern hemisphere. If the topographic gradient is reversed, a cyclonic circulation is produced.

[6] Four selected satellite sea surface temperature (SST) images from the Modular Ocean Data Assimilation System (MODAS) are displayed in Figure 3. These pictures show some obvious upwelling events characterized by a cold water center about 2° colder than the surrounding area, but the upwelling events cannot be always observed by satellite SST pictures when carefully checking all the pictures in summer. Predominantly, the centers of cold water are located in the northeast of Hainan. When checking the relevant summer SST images from 2002 to 2006, we find that the upwelling cannot always be observed. This is a phenomenon occuring at the central Vietnamese coast, which in summer is also a typical Ekman upwelling area [*Dippner et al.*, 2007]. The major problem using satellite SST images to detect upwelling is that they only give information about the near sea surface layer. In summer, the strong heat flux causes a strong stratification in the surface layer, which in many cases mask the upwelling from deeper layers. However, the SST images still show several centers of cold water distributed as 'patches'. Several questions are prompted on the basis of these satellite pictures: What are the main factors controlling the upwelling strength? Why are there several upwelling areas distributed as patches but not a single large upwelling region along the coast? Why is the upwelling not persistent like the wind is in summer which forces the Ekman driven upwelling? We set up a 3D high-resolution model to understand the upwelling dynamics in this open shelf region, and we focus on the results in June 2003, which refers to Figure 3b. In particular, we try to detect the role of topography and coastline shape in the wind driven upwelling system. In section 2 the model is described and the setup is explained. The model results of the standard control run are given in section 3, the numerical studies concerning the effects of topography and wind are shown in section 4, followed by the discussion in section 5 and the conclusions in section 6.

2. Data and Methods

2.1. Model Description and Configuration

[7] A high-resolution 3-D baroclinic, free surface model, HAMburg Shelf Ocean Model (HAMSOM), [*Backhaus*, 1985; *Pohlmann*, 1996a, 1996b] was used to study the upwelling system. The model was applied to the SCS to study the general circulation for the first time in the eighties [*Pohlmann*, 1987]. The nested technique was used in the northwestern part of the SCS (Figure 1). Hourly data of sea

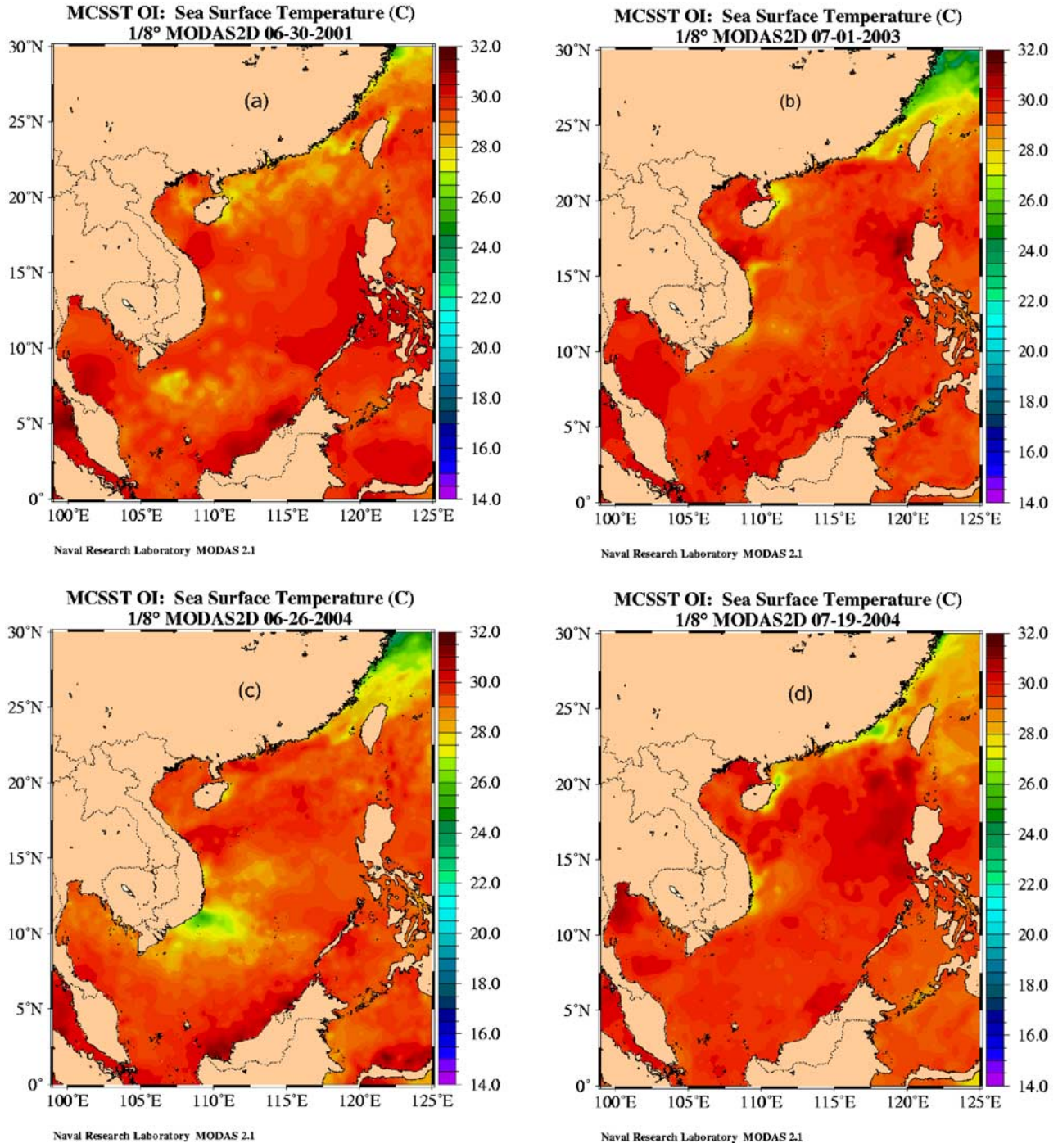

Figure 3. Satellite pictures of SST (°C) from MODAS in summer. They cover the region of the entire SCS on (a) 30 June 2001, (b) 1 July 2003, (c) 26 June 2004, and (d) 19 July 2004. The pictures can be downloaded from http://www7320.nrlssc.navy.mil/modas/. We select the pictures which show the obvious upwelling events (yellow or green color) in eastern Hainan but most of satellite pictures do not show this signal.

surface elevation at open boundaries was provided by a large-scale version of HAMSOM covering the entire SCS with a resolution of 7.4 km [*Hein*, 2007]. The general model configuration, boundary conditions, and parallelization of the code were identical to that used by *Pohlmann* [2006].

[8] To minimize the influence of open boundary, the open boundaries are at least 3 degrees away from the area of interest. The model domain is located between 15°–22°10′N, and 105°30′–113°30′E using a fine resolution of 1′ which allows to resolve the mesoscale processes on the shelf. In this model the time step is 300 seconds which is appropriate for 1 min spatial resolution. Tidal processes are neglected in this study since the tidal-induced upwelling mainly induced by eddies only plays a minor role in this region [*Lee et al.*, 1999]. The *z*-coordinate system is applied

in the vertical direction using a maximum of 24 layers. The resolution in the upper 50 m is 5 m, the layers between 50 m to 150 m have 10 m thickness, and the other layers are located in 170 m, 200 m, 300 m, 1000 m depth. The model is forced by meteorological reanalysis data which is provided by NCAR/NCEP [*Kalnay et al.*, 1996]. The resolution of the forcing data is 2.5° in zonal and meridional directions and 6 hours in time. One may doubt if this coarse spatial resolution forcing is able to reproduce small-scale coastal features like eddies and frontal variability adequately. However, the large-scale wind field is responsible for the Ekman induced upwelling whereas the small-scale local wind stress curl plays a relatively important role on the modification of the large-scale features [*Enriquez and Friehe*, 1995]. Therefore, the coarseness of the forcing can be accepted, since the dominant part of the wind induced upwelling is resolved.

[9] The initial temperature and salinity fields are obtained from the climatological LEVITUS data set [*Levitus et al.*, 1994]. The spin-up is performed by rerunning the year 2000 twice using the atmospheric forcing of 2000. Subsequently the final elevation, velocity, temperature and salinity fields are stored to be used as initial conditions. The actual model run is performed for the years from 2000 to 2006 in order to study the interannual variability of the upwelling. For the experiments, we have chosen the year 2003 since the anticyclonic circulation is strongest compared to other years, and there is no counter flow in the northern SCS shelf, i.e., the variability of upwelling areas is smaller than in normal years [*Hein*, 2007]. From satellite picture (Figure 3b), there occurred strong upwelling on 1 July 2003, so we present the model results in June. In this study we aim to understand the upwelling mechanisms, not the perfect reproduction of an actual situation. This should be the next step after we obtained a sufficient understanding of the exact dynamics in this region. Therefore, it is not necessary to compare model results with satellite SST or cruise data quantitatively to estimate the actual model error. Accounting for these constraints, a qualitative comparison of the model results with observations seems to be the appropriate way in this paper.

2.2. Satellite Remote Sensing Images

[10] The satellite images presented in this paper are based on the newly available data from the Modular Ocean Data Analysis System (MODAS) [*Kara and Barron*, 2007]. The high-resolution 1/8° daily MODAS SST product is mainly based on Advanced Very High Resolution Radiometer (AVHRR) satellite measurements. MODAS SST is a purely satellite-based product, which does not include in situ data. But for the validation analysis 219 permanent daily SST time series from both coastal and open ocean buoys distributed over the global ocean are employed [*Barron and Kara*, 2006]. This product is used to obtain a synoptic overview over the different upwelling areas and the involved variability in the strength of upwelling events in different months (Figure 3).

2.3. Cruise Observations

[11] To detect the spatial and temporal variability in the east Hainan upwelling area, a cruise has been carried out from 19 to 22 August mainly in area 3 (Figure 2). CTD data, current meter data, and chemical parameters were measured, temperature and salinity data were measured with a SeaBird SB19 CTD system at each station.

[12] Five sections have been selected that run perpendicular to the coastlines, covering the area from Tung-ku Chiao to Ta-hua Chiao where the upwelling always occurs in summer. The temperature distribution in Section T1 shows a stratification at 20 m depth at the near coastal station and at 50 m depth at the offshore station, respectively (Figure 4a). Obviously, the strongest upwelling has been observed at section T1. Even in this situation the upwelling was not reaching the sea surface because the strong atmospheric heat flux was dominating the 5 m surface layer. At section T2, the isotherms approached the surface close to the coast, where a cold water center of 27°C was produced (Figure 4b).

[13] When we look at the SST distribution during the cruise, the cold water center (26°C) was located in the near coastal station of section T5 (Figure 4c), whereas the bottom temperature distribution showed that the warm water center (>25°C) can be found at the near coastal station of section T2 (Figure 4d). Since the isobaths were running parallel to the coastline in the observational region, the warm water center could not be caused by differential heating because of the shallowness of the area. In the observation, we found a dipole structure, i.e., an upwelling center behind a cape while a downwelling center exists in front of a cape looking in the direction of the flow. This can be confirmed by our modeling studies for this area, where we also found a similar structure around the capes. The formation of this dipole structure was closely related to the topographic effects, which are discussed in section 5.

3. Results (Control Run)

3.1. Upwelling Centers Based on the Model Results

[14] Looking at the results of the year 2003, we find that upwelling was the strongest in June and July, and there occurred a strong upwelling from satellite picture on 1 July (Figure 3b). So we analyzed the model results from 1 June to 30 June under standard conditions and defined this as the control run. For understanding the principle dynamics of upwelling, this 1 month period turned out to be enough. We show the model results of SST, velocity and vertical velocity every 5 days in order to study the temporal evolution of the upwelling (Figures 5–7). Velocity fields at 30 m depth are presented because they coincide with the average depth of the thermocline. Understanding the processes in this layer helps to study the lifting of the thermocline, which is a major phenomenon related to upwelling. It has to be noted that in coastal areas, the current at 30 m depth already represents the bottom current. Vertical velocity fields at 10 m are shown to represent the vertical velocity close to surface.

[15] Figure 5 shows the model SST results. Upwelling cannot be detected during the first 5 days (Figure 5a). There are three cold water centers on 10 June (Figure 5b), which are located in the north of three capes, in area 1, 2 and 3. These three centers are closely related to the shape of the coastline which can be proved by the velocity fields in 30 m depth (Figure 6b). The cold centers are also connected to the consistent southwesterly wind (Figures 8a and 8b) because

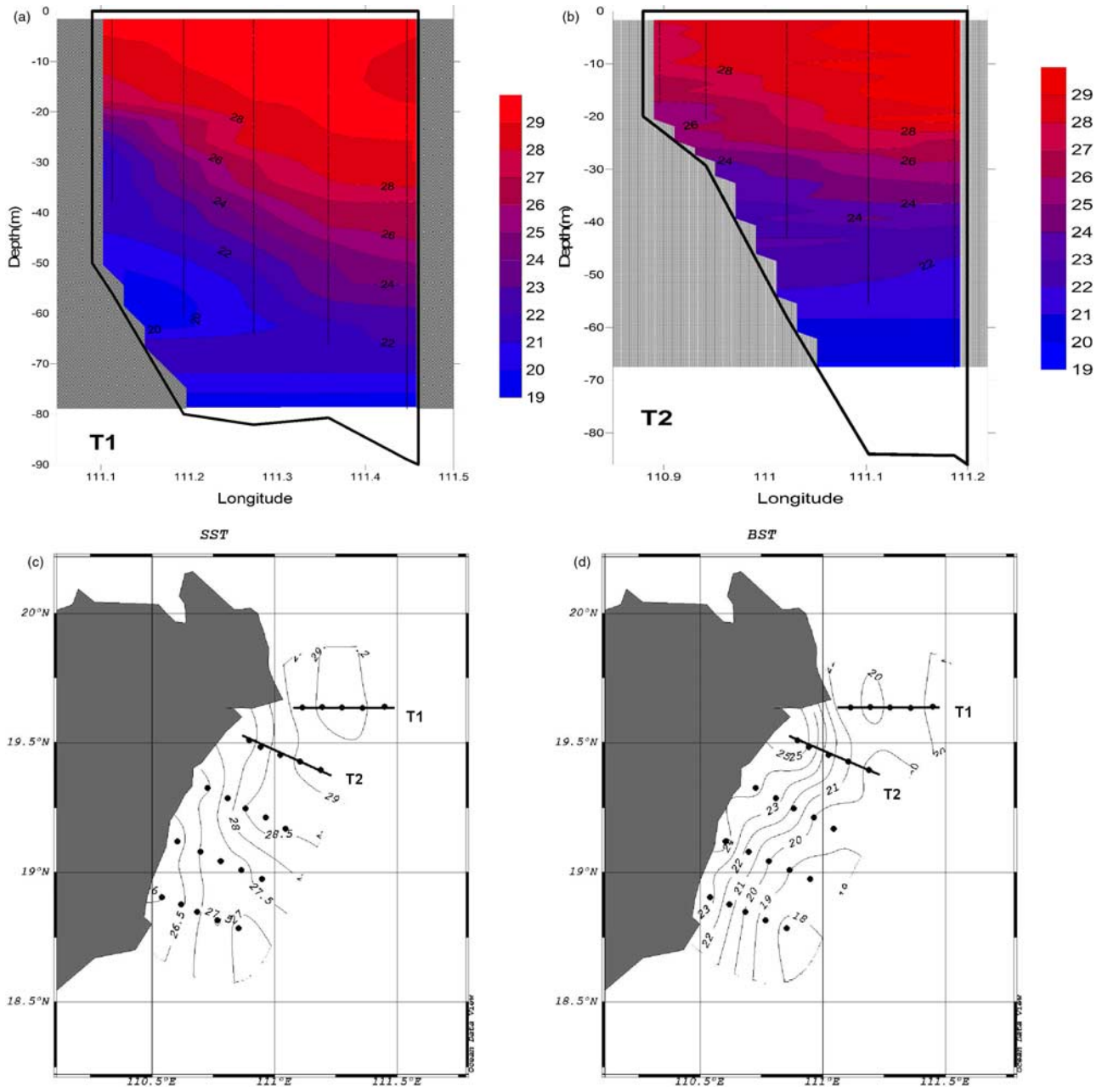

Figure 4. Observed temperature (°C) distribution along section (a) T1 and (b) T2 during the cruise in August 2007. The dotted lines show the exact observation locations. The observed (c) SST and (d) bottom temperature during the same cruise. The black dots indicate the monitoring stations.

north of these capes is downwind. If we carefully check the circulation in all three bays in areas 1–3, the currents behind the cape point toward onshore and by this cause an upwelling in the cape area. This is confirmed by the vertical velocity fields showing that the maximum of the vertical velocity is exactly located in the cape area (Figure 7b). The maximum upward velocity is 3×10^{-4} m s^{-1}. On 15 June, the velocity field in area 3 shows a counter flow in the inner bay (Figure 6c), which causes a blocking of the upwelling (Figure 5c), and weaker currents than other days. This development coincides with a change in wind direction from southwesterly to easterly (Figure 8c), indicating that the locally varying wind stress has a strong influence on the strength of the upwelling. This wind relaxation will be discussed in section 5.1. The same counter flow structure can be found also for 20 June in area 2 (Figure 5d), although the wind direction is changed back to southwest. The counter flow also decreases the upwelling (Figure 6d), moreover, the main axis of the bottom currents on 15 and 20 June is not as close to the coast as on the other days. Therefore, in this case the adjustment of the current to the change of the wind direction takes about 1 week. The strongest upwelling of the month can be found on 25 June. Besides the above mentioned areas 1–3, the upwelling occurs also in area 4 (Figure 5e). The main axis of the bottom currents is

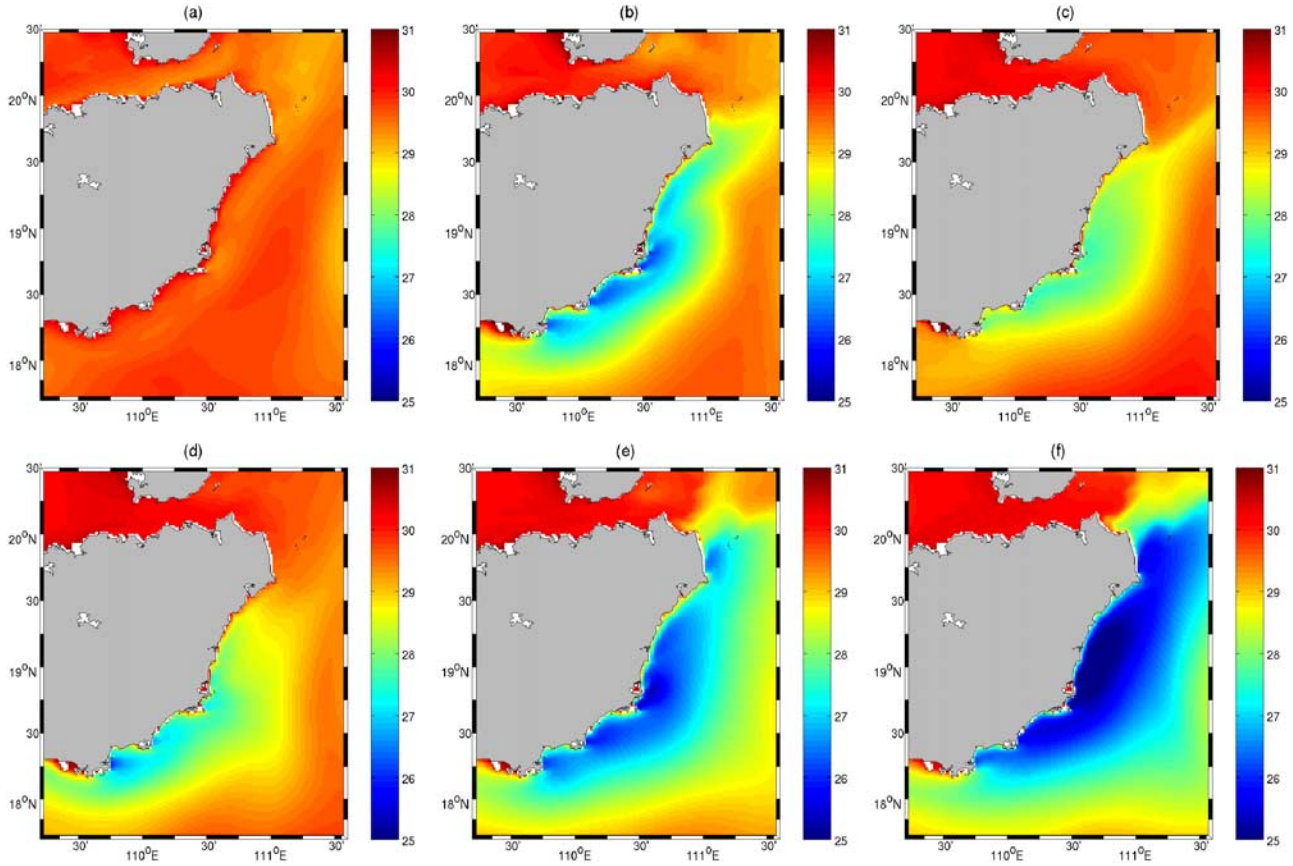

Figure 5. Simulated SST (°C) distribution east of Hainan Island on (a) 5, (b) 10, (c) 15, (d) 20, (e) 25, and (f) 30 June 2003 (control run). The temperature in the cold water center is about 25°C, and the largest upwelling event occurred on 30 June (Figure 5f).

close to the coast at this date (Figure 6e). After this strong upwelling event, the strength of onshore currents decreases because the water elevation of the coastal area is comparatively high. This weakens the upwelling center considerably followed by a subsequent advection away from the coast (Figure 6f). The wind direction on this date is southeast, which may also influence the movement of the upwelling center (Figure 8f). Although on this date we still can observe large areas of cold water in the surface layer (Figure 5f), the vertical velocity shows already a downwelling in the coastal areas (Figure 7f), which indicates that the large area of cold water is caused by horizontal advection. Interestingly, the two strong wind events on 10 and 25 June lead to totally different distributions of SST, which is certainly influenced by wind strength, but we also think there are other effects which can be explained by the momentum balance as discussed in section 3.3.

[16] With our high-resolution model, we find that the location and strength of the upwelling centers within 1 month may change very quickly, which may be related to baroclinic instabilities of the upwelling front and fluctuations of the southwesterly wind. Our results reveal that the main mechanism responsible for the upwelling events is wind, but topography plays an important role in the formation of the uneven distribution of upwelling centers.

[17] In area 4, a resistant cold cyclonic eddy can be found (Figure 6) at 30 m depth, but the vertical velocity related to this eddy even indicates downwelling at the end of the month, probably because of the interaction with the rough topography. The cold current from the Qiongzhou Strait flows northward after leaving the strait. Thus, there is no connection between the Qiongzhou Strait water and the cold water in area 4, which could explain the cold eddy.

3.2. Cross-Shelf Structure

[18] In summer, the thermocline is always present in all the sections from west to east (Figure 9). This fits with our assumption that surface fluxes heat up the sea surface producing the strong stratification, and only strong upwelling can weaken the thermocline. The temperature structure in these sections indicates the strength of upwelling for 4 different areas. Interestingly, the lifting of the isotherms can occur more than 100 km away from the coast (Figure 9c).

[19] The model results qualitatively also agree with observations mentioned above. The observed surface water exhibits about 30°C, at the thermocline the temperature is about 20°C and the upwelled water is about 26°C (Figures 4 and 9). These main features of upwelling are well captured by the model which indicates reasonable model performance.

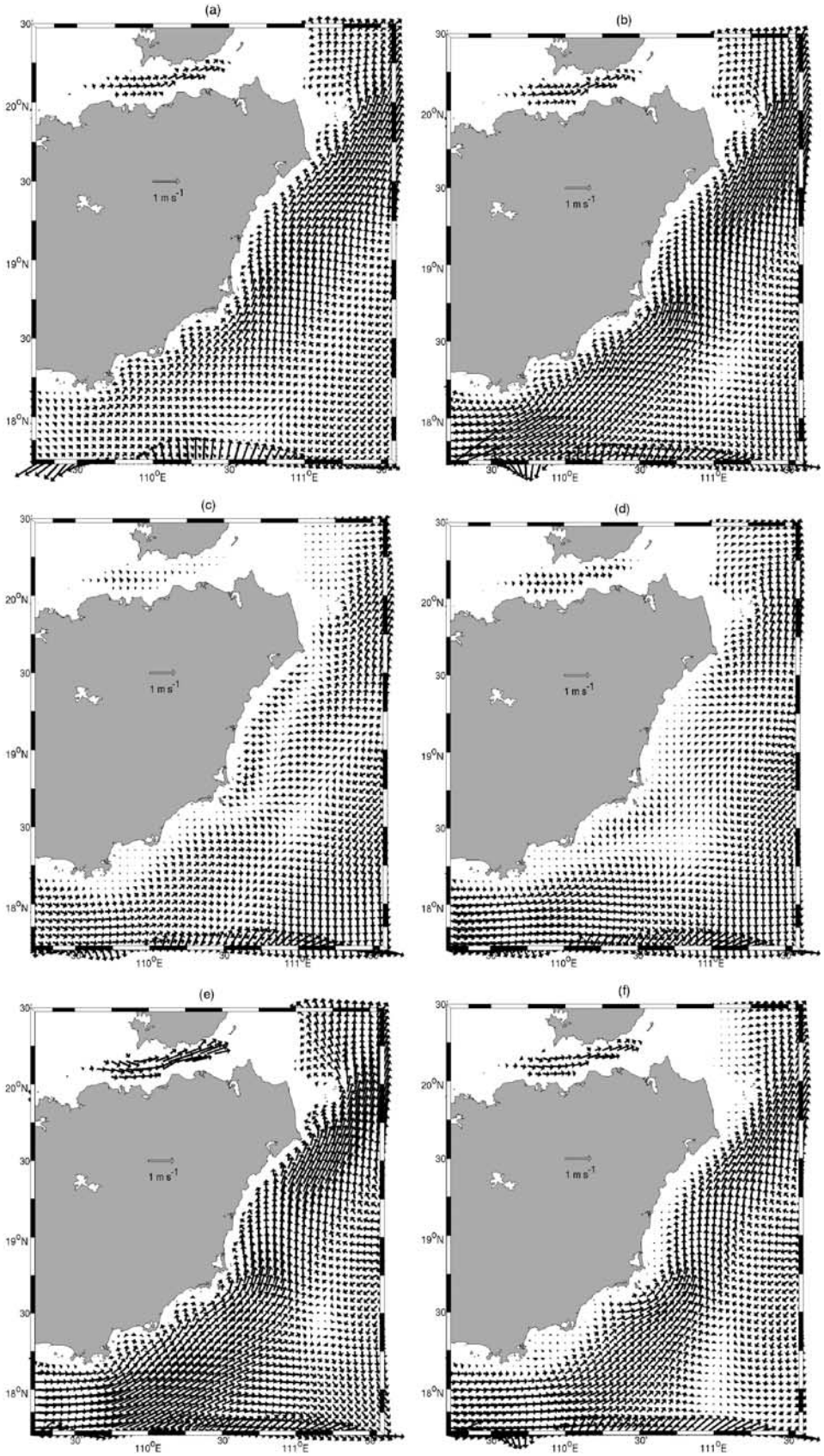

Figure 6. Daily average current fields (m s^{-1}) at 30 m which represent the subthermocline flows on (a) 5, (b) 10, (c) 15, (d) 20, (e) 25, and (f) 30 June 2003 (control run). The velocity is plotted at every third grid point. There occur counter flows in the northern inner bay on 15 June (Figure 6c), 20 June (Figure 6d), and the main axis of the bottom currents run close to the coast on 25 June (Figure 6e).

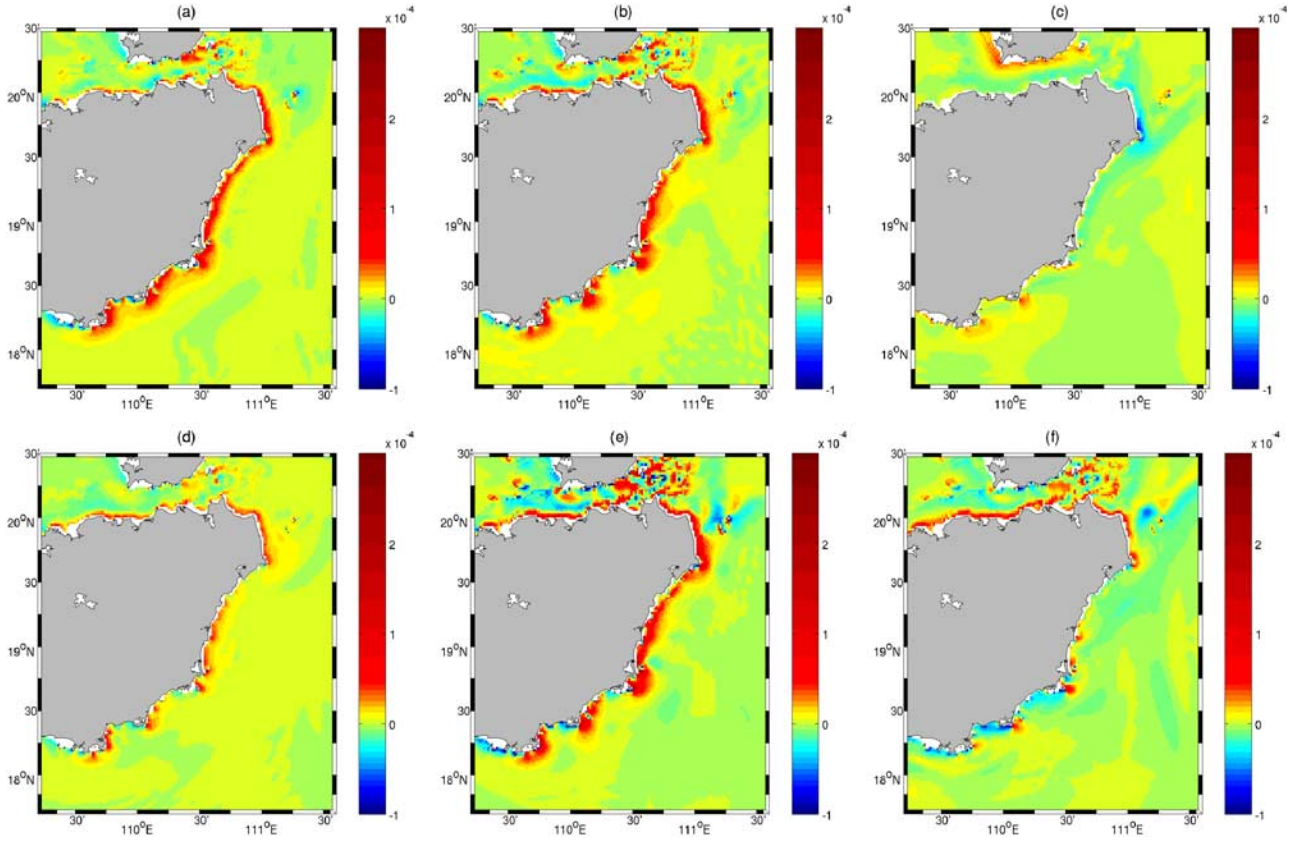

Figure 7. Vertical velocity fields (m s^{-1}) in 10 m depth on (a) 5, (b) 10, (c) 15, (d) 20, (e) 25, and (f) 30 June 2003 (control run). The positive direction of vertical velocity is upward. There is always a dipole structure around the cape with an up- and downwelling center.

[20] The upwelling development differs from section to section, we found the upwelling first starting at section S1 and S2 (Figures 9a and 9b), while after 20 June it started at section S3 and S4 (Figures 9c and 9d). A density gradient toward the along-shore downstream direction is formed because of the upwelling. This gradient forces an along-shore density-induced current, which pushes the cold water toward the north and east. The result of this process is an enhanced upwelling which can be found from SST distribution (Figure 5f).

[21] When studying the origin of the upwelled water, it is obvious that at all the sections the upwelled water comes from 30 m to 40 m depth. This indicates that there is a threshold for the available energy to lift the thermocline upward. It is also clear that the lifting of the thermocline in the northern section (area 4) needs more energy because of the wider shelf compared to area 3, where less energy is dissipated. This agrees with our observations from section T1. The occurrence of a cold water patch in area 4 often observed by satellite can probably be attributed to a Taylor column developing over a shallow bank [*Chapman and Haidvogel*, 1992; *Davies*, 2006].

3.3. Momentum Balances

[22] We calculate the momentum balance in the zonal and meridional directions at the 20 m isobath in area 3 (Figure 2), using a method similar to that of *Weisberg et al.* [2001]. There occurred obviously two wind events in this period, the first one from 1 to 13 June, and the second from 18 to 30 June, whereby the second event is more constant over the entire period. In the following, we assume that the zonal direction can present the cross-shelf direction. In this direction, wind stress is the leading term which causes the cross-shore pressure gradient, the Coriolis acceleration and the nonlinear term to balance it (Figure 10a). As discussed in section 4.1, the nonlinear term is an important ageostrophic contribution in the cross-shelf direction. We also find that the response of the pressure gradient and other terms to the wind is very quick in both directions, i.e., about half a day delay in the zonal direction and less than half a day delay in the meridional direction. In the meridional direction, wind is also the leading term forming an along-shore pressure gradient, but it seems that the ageostrophic contribution is more significant in this direction since the Coriolis term is not comparable to the along-shore pressure gradient (Figure 10b).

[23] During the first wind event, the change of the pressure gradient term fully compensates the wind stress term, but during the second period there is another term influencing the pressure gradient which should be the baroclinic pressure gradient. From this difference we can explain the different SST distributions after the two wind periods. After the first wind period, the wind is weak and the pressure gradient decreases following the wind stress, therefore we could not find any decrease in SST after this wind period. The upwelled water, however, remains below

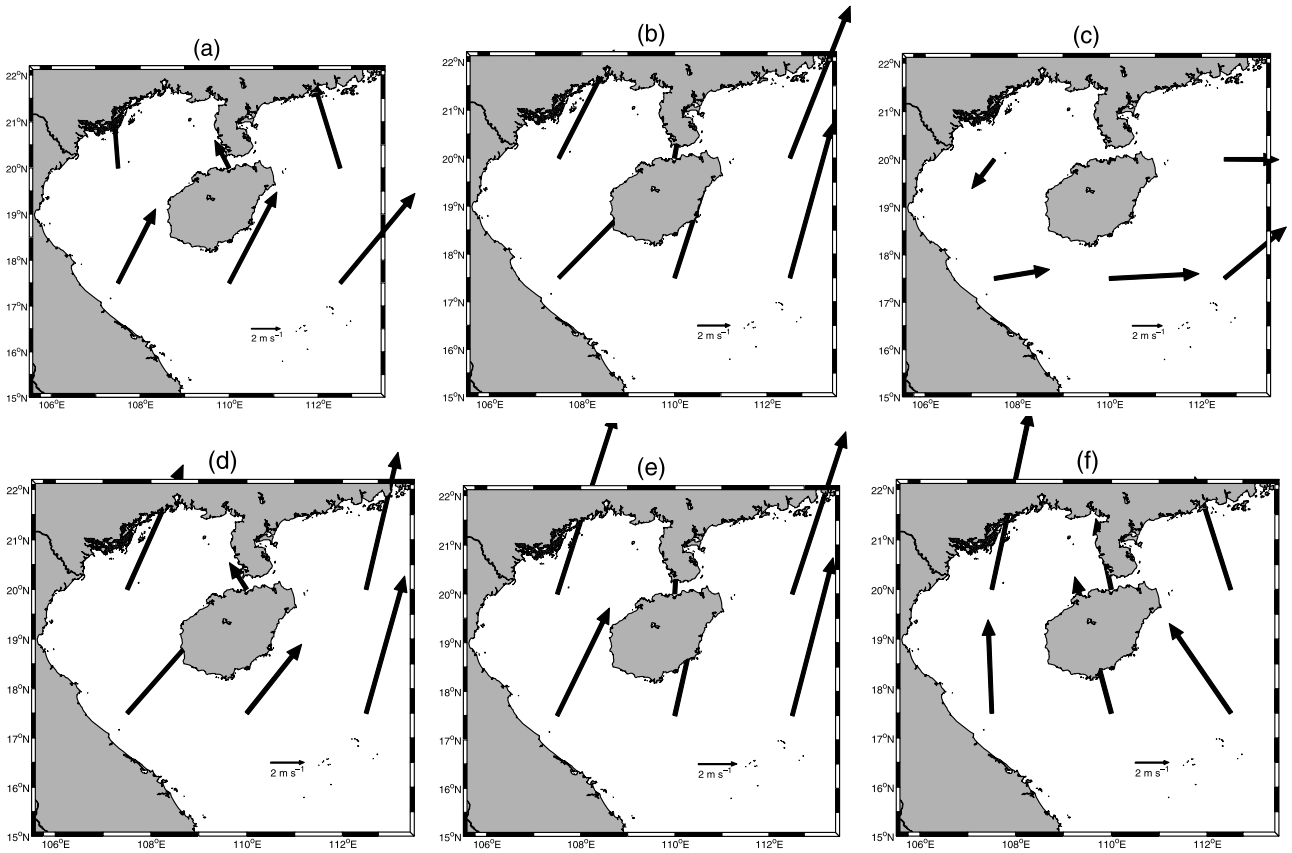

Figure 8. Sea surface wind fields (m s^{-1}) from NCAR/NCEP reanalysis data on (a) 5, (b) 10, (c) 15, (d) 20, (e) 25, and (f) 30 June 2003. The resolution of NCEP data is 2.5°.

the surface, which could be seen in cross-section temperature distribution (Figure 4a, S3). During the second wind period, the wind lasts longer than during first wind event, and hence the upwelling centers with their induced density variation can form in this period. The combined wind and density effects cause the subsequent horizontal advection of the upwelling centers. Because of the preconditionary by the first wind event and the length of the second wind event, only after second upwelling event we can identify a large upwelling area in the SST distribution which also coincides with satellite observations (Figure 3b). This study helps us to understand why upwelling cannot always be observed from satellite pictures, when upwelling favorable wind conditions are prevailing.

3.4. Mixing Processes at the Shelf Break

[24] The vertical mixing process is important when the upwelled water reaches the surface mixed layer. When the boundary current passes one of the capes, it is accelerated because of the funneling effect. Here we have chosen one snapshot showing the turbulent viscosity coefficient (A_V) at 20 m depth on 22 June before the strongest upwelling. In the coastal area, the maximum value of A_V is found at a latitude of about 18°30′ N (Figure 11) where the currents cross over the ridge in the vicinity of the cape. When the current flows along the cape, it is accelerated by topographic funneling which leads to high A_V values in this area (Figure 6).

[25] Internal waves have been reported in the northern SCS shelf break by collecting satellite images and *in situ* data [*Hsu and Liu*, 2000; *Orr and Mignerey*, 2003]. *Hsu and Liu* [2000] also reported the internal waves at the east Hainan shelf break. On 22 June, the distribution of A_V shows a wave-like pattern at the shelf slope in area 3 (Figure 11 (left)), which indicates an internal wave which is generated at the shelf break. When we check the temperature distribution in section of 19°N, the thermocline also shows a wave pattern with several wave lengths at 20–30 m depth (Figure 11 (right)). In most cases, the nonlinear internal tide is the primary generation mechanism for nonlinear internal waves. However, we did not include tide in the model which implies that the energy of internal waves is generated by surface winds and buoyancy forcing in the SCS.

[26] Another area which shows high A_V values is the northeastern corner of Hainan Island (area 4). We find that the location of the high values exactly coincides with the location of a small bank (Figure 2). This small bank also plays an important role since it generates cyclonic eddies which may keep the upwelled water from leaving to the open water, a typical feature if a Taylor column has developed.

4. Numerical Experiments

[27] As we already performed the control run to understand the basic features of the upwelling, we designed three

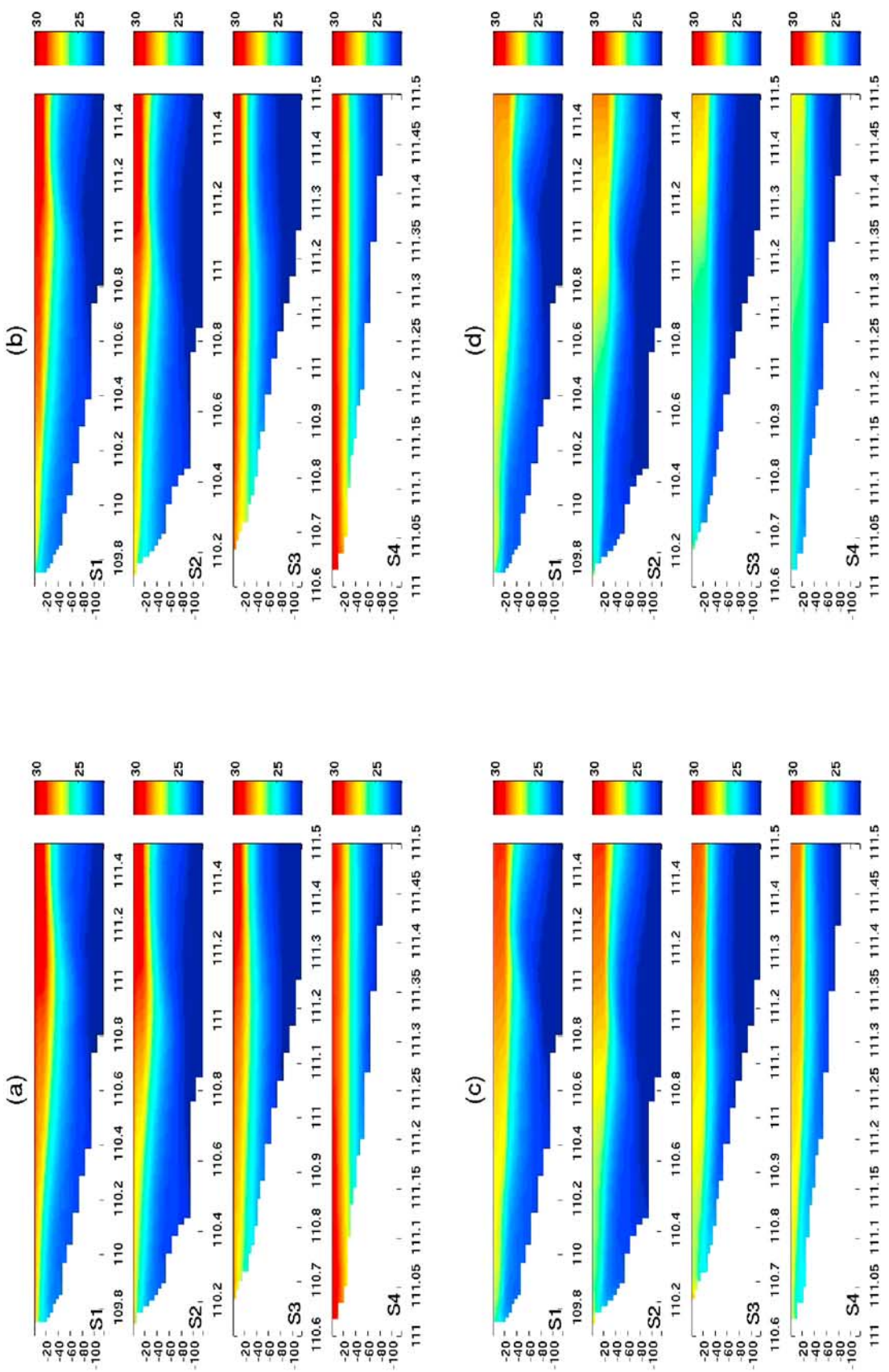

Figure 9. Temperature (°C) distribution simulated by control run at section S1, S2, S3, and S4 (Figure 1) on (a) 15, (b) 20, (c) 25, and (d) 30 June 2003. X axis is longitude, and Y axis is depth (m).

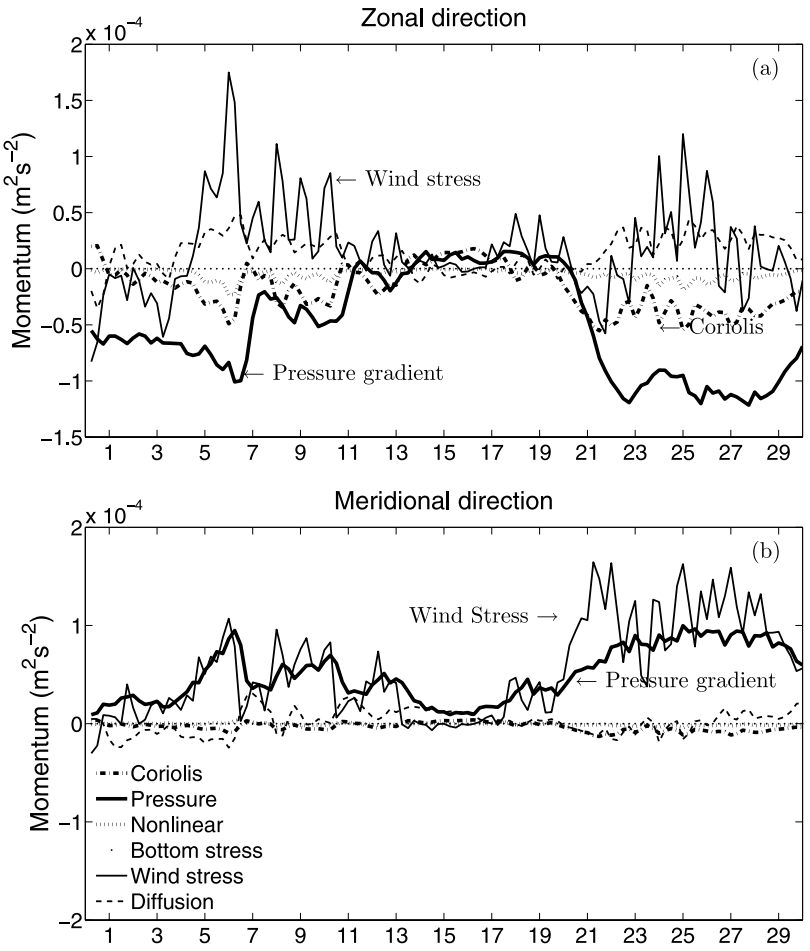

Figure 10. Simulated time series of the vertically integrated (a) zonal and (b) meridional momentum balance terms in June. They are sampled at the 20 m isobath in area 3. X axis is the day in June. The time tendency terms are not shown. Wind stresses are main forcing terms.

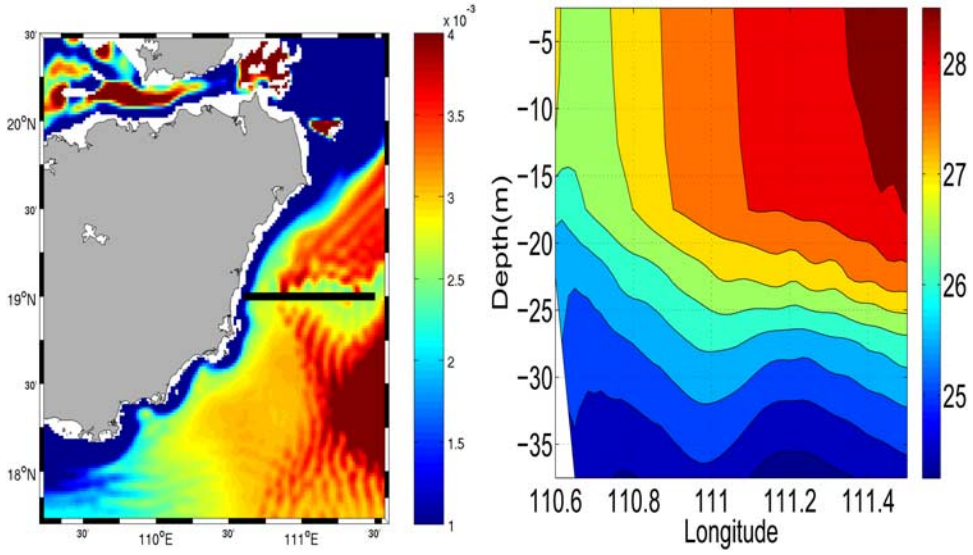

Figure 11. The distribution of the (left) turbulent diffusion coefficient ($m^2\ s^{-1}$) at 20 m depth and (right) temperature (°C) distribution in section of 19°N on 22 June. The model results are obtained from the control run. Here 22 June is the date before the strongest upwelling event. The distribution in the slope area shows a distinct wave pattern (red/yellow color) along the section. The temperature distribution in this section shows an internal wave formed in the slope area.

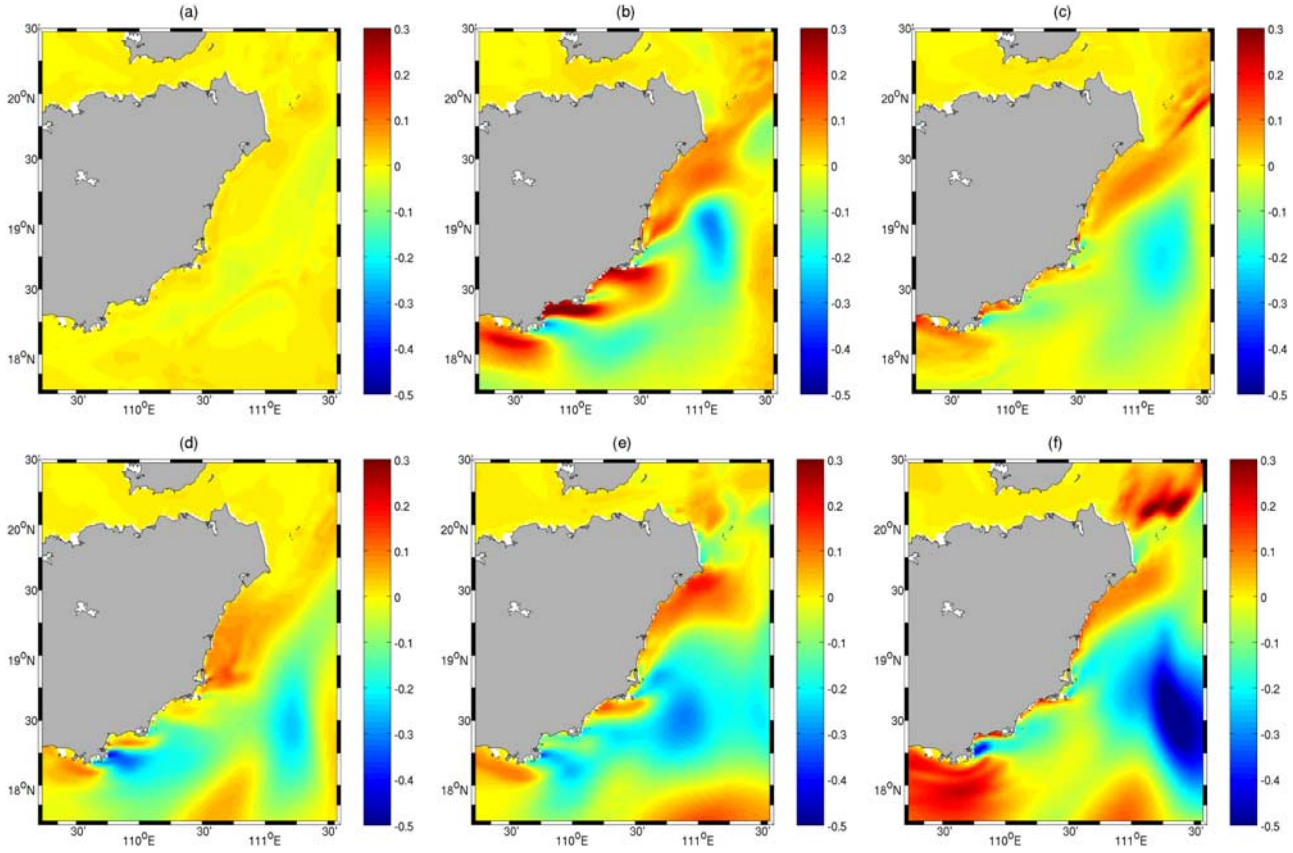

Figure 12. The model results show the SST (°C) difference ($SST_0 - SST_{exp}$) between the reference run (SST_0) and the nonlinear numerical experiments (SST_{exp}) on (a) 5, (b) 10, (c) 15, (d) 20, (e) 25, and (f) 30 June. In the coastal area, the evolving dipole structures indicate the strengthening of both up- and downwelling.

experiments to elucidate more details of the dynamics. All of these runs have been carried out for a 1 month period. In section 4.1, an experiment is performed to study the effect of nonlinear terms. In section 4.2, 9 experiments with different wind directions are conducted to study the role of wind in the upwelling system. In section 4.3, the experiment using artificial topography is performed to investigate the influence of topography in more detail.

4.1. Nonlinear Effects

[28] In this sensitivity study the nonlinear terms are removed from the momentum equations, whereas all the other terms are kept the same as in the control run. The difference of SST_{exp} (SST of nonlinear experiment) and SST_0 (SST of control run) are shown in Figure 12. The effect of the nonlinear terms becomes larger within 10 days and can be observed on 10 June (Figure 12b) when the strong upwelling occurs. After 1 month, SST in the area about 40–50 km away from the coast increases by more than 0.5°C. On 25 June, the SST's near the capes in areas 1–4 all show an increase which indicates a strengthening of upwelling by nonlinear effects.

[29] Throughout the month, the difference in SST along the main axis of the current increases, whereby the biggest increase occurs between 18°30′N and 19°N. But in the near coastal area, the effect of the nonlinear terms is quite complicated and also shows a dipole structure: (1) the SST increases exactly at the cape areas and (2) there are coastal water masses colder than the control run, especially south of the capes (Figure 12). The results of the experiment indicate that nonlinear effects strengthen both upwelling and downwelling in the coastal area.

[30] The effect of the nonlinear terms is the strongest at the shelf break, without the nonlinear term, the main currents less strongly intrude into the shelf area because of inertia, and there is less interaction between open ocean and shelf. The temperature differences of the layer 30–40 m which is below the thermocline exhibit the most significant influence of the nonlinear effect (Figures 13c and 13d), whereas in upper layers the influence is more closely related to the coastline shape (Figures 13a and 13b).

4.2. Wind Experiments

[31] Experiments using different wind forcing in the overall modeling area are performed. The experiments are not only intended to test Ekman theory in the study area, but also to show the role of topography in the upwelling system under a constant wind. The initial conditions of the experiments are all the same as chosen for the standard run, and the simulation period for each experiment is also 1 month. Firstly, we tested one case without any wind forcing, which results in no cold water center in the entire domain

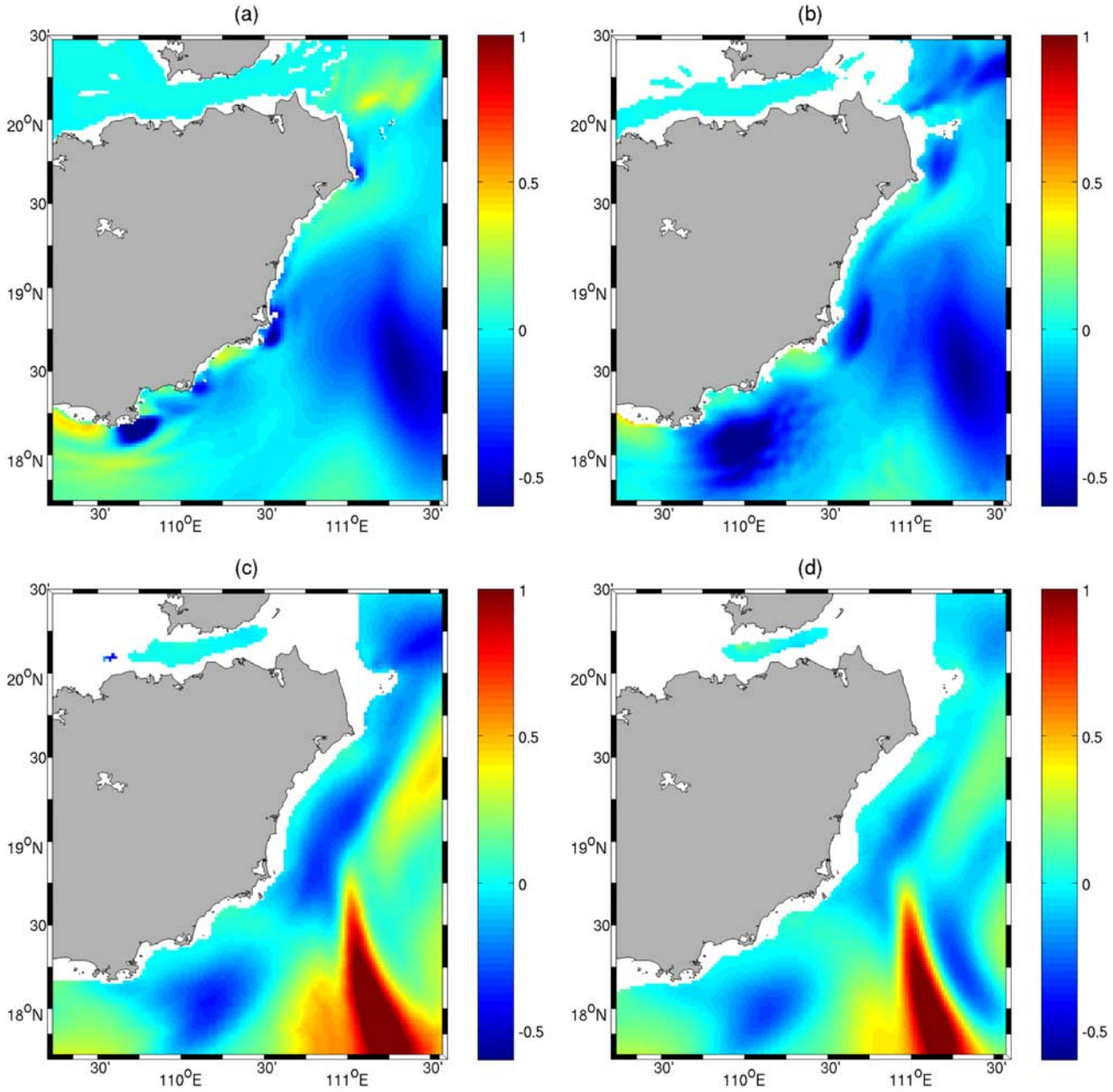

Figure 13. The model results of temperature (°C) differences ($T_0 - T_{exp}$) from the nonlinear numerical experiments at layer (a) 10, (b) 20, (c) 30,and (d) 40 m on 30 June.

(Figure 14). Then, we choose eight wind directions expressed according to the meteorological convention, i.e., North(N), Northeast(NE), East(E), Southeast(SE), South(S), Southwest(SW), West(W) and Northwest(NW) with a wind speed of 5 m/s to force eight different experiments.

[32] The strongest upwelling occurs in the SW case. The upwelling favorable wind directions for area 1 are W and SW winds, for area 2 a SW wind and for area 3 SW and S winds (Figure 14). Therefore, the strength of upwelling should mainly depend on the frequency of southwesterly wind. Southerly winds play only an important role for upwelling in areas 3 and 4. It is interesting to note that after 1 month the strength of upwelling even in the strongest upwelling case (SW wind) is much smaller than in the standard run (Figure 5f). The main reason for this is the fact that the wind from 20 to 30 June exceeds 5 m/s by up to about 7 m/s (Figure 8).

[33] In the SW and S experiment, after a continuous Ekman transport for 1 month, the upwelling cores still show patterns of patches rather than an extended homogenous structure, especially in areas 1 and 2. Under the natural wind condition, the relaxation of wind produces rapid hydrographic changes of the shelf circulation [*Rosenfeld et al.*, 1994]. The relaxation here refers to the reduction or reversal of the upwelling favorable wind stress, which is already found in the wind data (Figure 8c) and the corresponding circulation changes (Figure 6c) during the simulation. When the relaxation is ignored in the experiments, we still can find

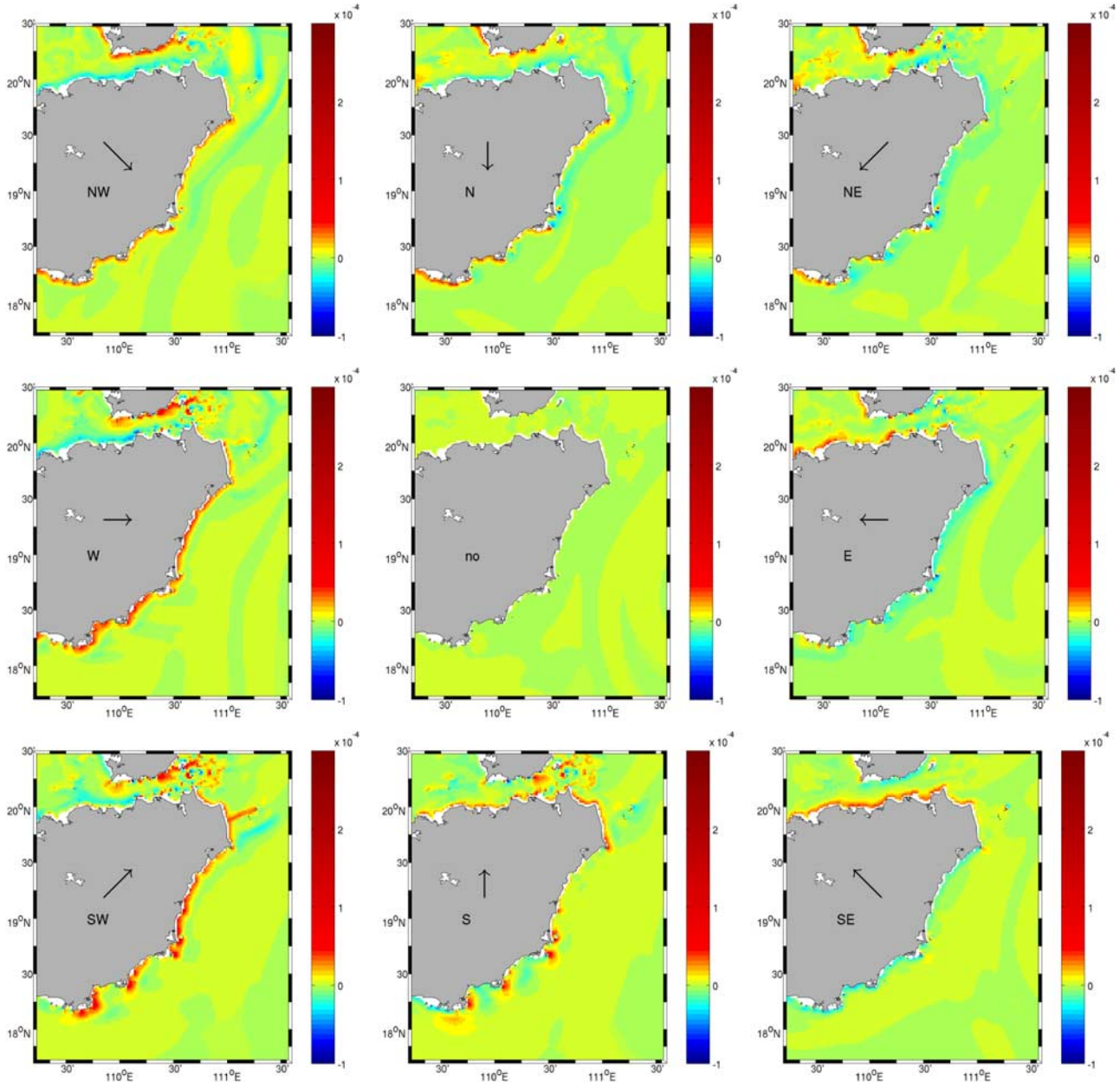

Figure 14. The model results of vertical velocity (m s^{-1}) at 10 m obtained from numerical experiments with different wind directions expressed according to the meteorological convention; they are NW, N, NE, W, E, SW, S, SE, and no wind case. Each wind experiment run lasted for 1 month.

the upwelling centers near capes. It is obvious that topography plays a more important role than the pure Ekman transport in the formation of the upwelling centers in area 1 and 2 [*Song et al.*, 2001].

4.3. Topographic Experiments

[34] As satellite images show, a frequent upwelling area is located between Ling-shui Chiao and Tung-ku Chiao (area 3), where there are several bays connected to each other. In this area, the shelf is narrow, thus cold water can easily intrude into the coastal area. In the southern part near Chin-mu Chiao (area 1) and the northern part (area 4), the shelf is wider than in area 3 (Figure 2), so cold water cannot enter the coast shelf as easy as in area 3. The dipole structures in area 1 and 2 are quite obvious. Therefore, we want to analyze the impact of topographic variations in area 1 and 2 on the upwelling processes in following experiment.

[35] For this purpose, the bays in area 1 and 2 are filled in this experiment, and the currents can only pass along the shelf slope (Figure 15). Compared to the control run, the strength of upwelling does not show a large difference in area 3, neither does the location of upwelling (Figure 15). Since the change of the coastline does not change the

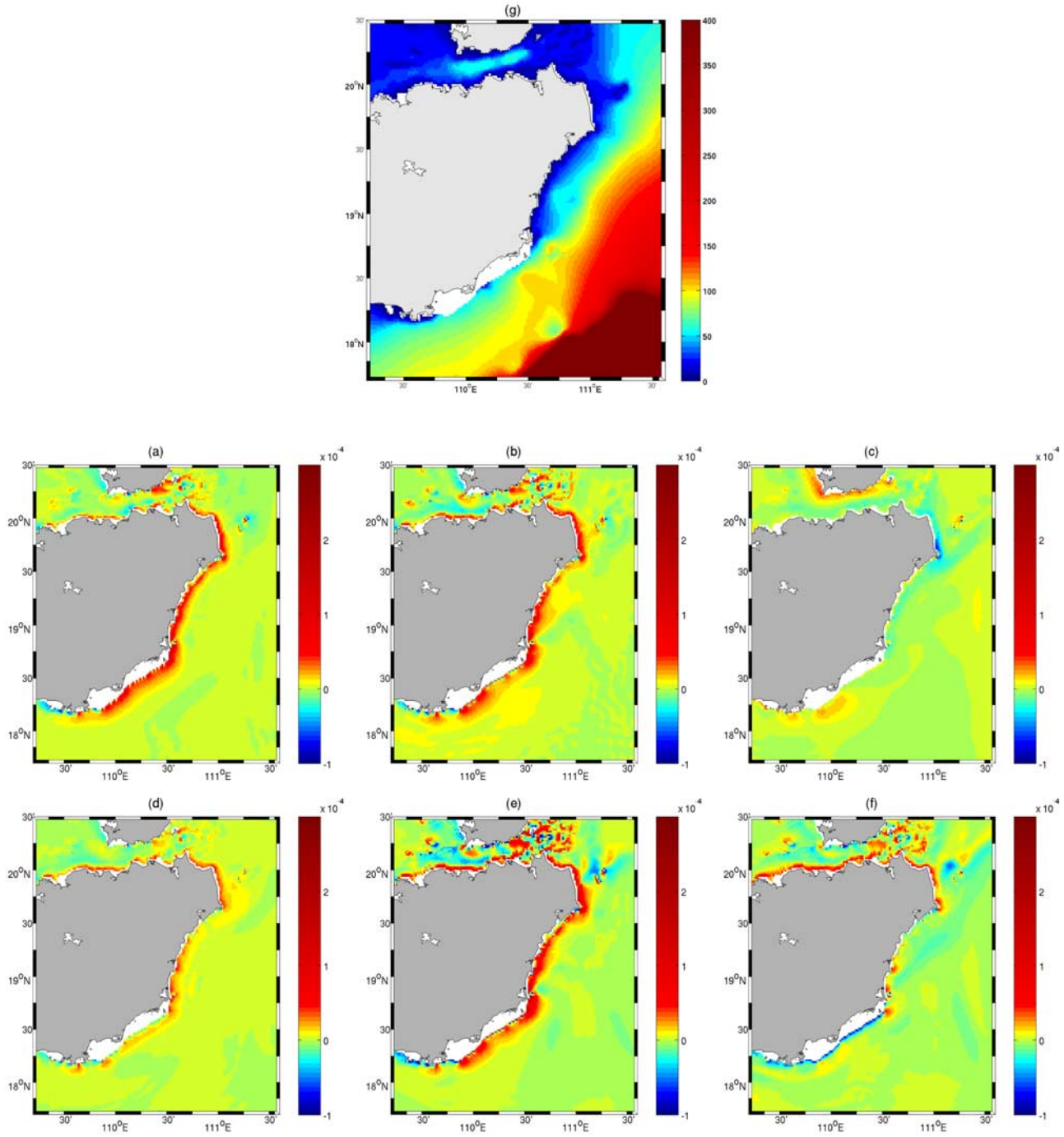

Figure 15. The model results of vertical velocity (m s^{-1}) at 10 m according to the topographic experiment on (a) 5, (b) 10, (c) 15, (d) 20, (e) 25, and (f) 30 June. (g) The modified topography of this experiment, i.e., the bays in area 1 and 2 are closed.

main current path and strength, it also gives the proof that the main upwelling dynamics in area 3 are BBL driven. The change of the shape of the coastline mainly induces local changes. Whereas in the control run the vertical velocity in shelf areas 1 and 2 indicates the combination of upwelling and downwelling centers around the capes, only upwelling centers are produced in this experiment. This indicates that the capes distort the potential vorticity balance which leads to localized up- and downwelling patches.

5. Discussion

5.1. Wind Effect

[36] On the basis of the model results, we found out that the factors controlling the upwelling east of Hainan Island are a composite of the large-scale circulation in the SCS,

and of wind and topography influences. Wind effects can be divided into the intensity of the wind stress over the large-scale basin of the SCS which drives part of the large-scale SCS circulation, the local wind variability that influences the cross-shelf pressure gradient and the locally varying wind stress curl. From previous modeling studies in the SCS, it is known that the wind stress and its ENSO related variability plays an important role in the large-scale SCS circulation, especially for the western boundary current [*Wang et al.*, 2006; *Chu et al.*, 1999], that also influences the circulation on the northern SCS shelf [*Su*, 2004]. The interannual variability of the western boundary current also influences the BBL currents east of Hainan Island, which decisively effects the formation of the upwelling in this region. In this paper we do not focus on the variability of the western boundary current itself which would complicate the discussion. From our model results, it is obvious that in area 3 the upwelling is mainly maintained by the BBL current. The upwelling is the strongest when the bottom currents are the closest to the coast which indicates the formation of current driven upwelling. The current-driven upwelling results in a density gradient that forces the currents back to the open ocean because of the geostrophic adjustment. This counter flow is evidence of geostrophic adjustment, which fits nicely into the BBL shutdown theory [*MacCready and Rhines*, 1993]. The impact of the local wind variability on the geostrophic adjustment is also obvious. The adjustment of the main current axis needs about one week if the wind direction changes. In this context, only one phenomenon is not directly clear: Why is there still an increase of the cold water plume near the surface toward 30 June, while the current fields and the vertical velocity fields both show no further upwelling signal?

[37] Firstly, when we check the current fields, there is no indication of a counter flow which means the BBL current keeps its strength. Secondly, the upwelling center is not located close to the coast, which can explain why there are no strong signals in the vertical velocity fields. But one can find a maximal vertical mixing off the slope, which can be one explanation for this cold water patch. This indicates that vertical mixing can play an important role in the upwelling system. Thirdly, the local wind direction also decisively influences the Ekman upwelling system, i.e., the upwelling in area 3 and 4 have a strong correlation with the easterly wind component. The experiments show that the Ekman-favorable winds are southwesterly and southerly. As discussed in section 3, the formation and strength of the patches of the upwelling system are mainly influenced by the frequency of winds from these two directions, but the locations of patches are determined by topographic features like capes and ridges.

[38] The locally varying wind stress can contribute to complicate the Ekman transport and upwelling. Firstly, it is shown that Ekman pumping due to local wind stress curl can be comparable to vertical transport by coastal Ekman transport [*Pickett and Paduan*, 2003; *Capet et al.*, 2004]. Secondly, changes in the orientation of wind stress relative to the local coastline lead to small-scale areas of higher upwelling and ''upwelling shadows'' [*Rosenfeld et al.*, 1994; *Graham and Largier*, 1997]. Thirdly, local gradients in wind stress and the resulting adjustments in coastal circulation produce along-shore pressure gradients that are largely responsible for undercurrents [*Dong and Oey*, 2005]. To gain a clearer understanding of how the small-scale wind stress influences the upwelling system, high-resolution atmospheric data is needed to give us a complete understanding in the surface Ekman layer. However, a discussion about the consideration of local wind effects is out of the scope of the present paper.

5.2. Role of Topography

[39] In the coastal ocean system, the wind forcing and topographic influence should be considered together while the momentum, energy and heat are absorbed by a relatively small volume of water because of the shallow water depth. For this study, the alongshore-varying topography obviously play an important role in the formation of upwelling. In cape areas a dipole of up- and downwelling areas can always be found both in model results, satellite pictures and laboratory experiments of *Narimousa and Maxworthy* [1986]. This phenomenon is a typical effect of topography. *Killworth* [1978] used a linear model to examine the effects on upwelling and Kelvin wave of a longshore varing topography. He discussed that the bottom condition leads to this dipole structure. This structure can be simulated by a theoretical study [*Song and Chao*, 2004]. They got the solution of the vertical velocity at bottom layer is related to along-shore topography variations. There is a downwelling on the upstream side of the cape and an upwelling on the downstream side. As shown in section 1, from the zeroth-order PV balance as discussed by *Yang and Price* [2000] we can also obtain the same distribution with a cyclonic circulation on the downstream side of a cape and anticyclonic circulation on the other side of the cape, which generate upwelling and downwelling, respectively (equation (2)).

[40] When upwelling favorable winds are strong enough, an SST anomaly is formed at the downstream of the cape, causing an upward lift of isopycnals toward the coast. The additional density induced pressure gradient will result in further movement of the upwelling center. Our model results reconfirm the solution of these previous theoretical model studies. The existence of several capes along such a short coastline is relatively exceptional, and thus the resulting number of patches of up- and downwelling is the dominant feature in these areas. So the main dynamics around these capes are topographically steered. This finding could be extended to other coastal areas which have similar complex coastlines.

[41] The impact of topography on this weak western boundary current system is proved by our numerical experiments. In general, the nonlinearity has a pronounced effect on a western boundary current, especially on the interaction between open ocean and shelf water. When the currents touch the wide southern shelf slope, the inertial part of the current is mostly dissipated, so the main effect of the nonlinear term shows up on the narrow shelf in area 3. This finding supports the conclusion that the main drivers of the dynamics in area 1 and 2 are interactions with the topography whereas in area 3 it is mainly a current driven process.

[42] Highlighting the topographic influence is not contradictory to the classical understanding of Ekman upwelling.

The classic Ekman theory considers only large-scale processes, whereas in a narrow upwelling system the topography can also play an important role. These smaller-scale processes might have a profound impact on the biology, chemistry and geology at similar scales.

5.3. Cold Water Center in the Northeast Corner

[43] In the northeastern corner of Hainan Island (area 4), a strong upwelling is frequently observed in satellite images (Figures 3b and 3d), which has been related to a stationary cyclonic eddy in summer [*Chai et al.*, 2001]. But in our model results, this cyclonic eddy is permanent throughout the entire simulation, it clearly has no strong relationship with temporally existing upwelling in area 4. Because the outflow from the Qiongzhou Strait does not influence this area, the water may also not originate from the Gulf of Tonkin. Therefore, we assume that this cold water remains cold originating from the shelf. A strong BBL current must advect the upwelled water to the northern shelf, whereas a cyclonic eddy helps to retain this cold water at the northeastern corner by means of a Taylor column, leading to a frequently observed feature.

6. Conclusions

[44] The upwelling in the east of Hainan Island is simulated by a 3D high-resolution hydrodynamic model. The main features of the upwelling, i.e., upwelling strength, and the temporal and spatial variation of upwelling centers, can be captured by the model. Because the net heat flux at the surface is relatively high in tropical areas in summer, a stable thermocline at 30–40 m depth developed. Upwelling can be deduced from the fact that the thermocline is lifted upward. From wind sensitivity experiments we conclude that the relaxation of southwesterly monsoon winds is one of the major factors influencing the variability of upwelling centers. For a complete understanding of the influence of the local wind stress on the upwelling, high-resolution atmospheric data are needed, their impact will be investigated in a future study. From the nonlinear experiments, we find the effect of the nonlinear terms is mainly confined to the shelf break, the interaction of open ocean and shelf weakens if we remove the nonlinear terms.

[45] The focus of the current study is on the along-shelf topographic variations which can also have a significant impact on the shelf circulation and from this on the upwelling. During summer monsoon, the western boundary current in the northern SCS changes its direction to the north. As a result, the along-shelf, near bottom current east of Hainan Island increases, resulting in an area of high bottom stress, which is responsible for an additional upwelling component. The uneven distribution of upwelling centers is caused by a combined effect of wind and topography. When the southerly or southwesterly wind is strong enough, topographic variations cause an upwelling center at the downstream side of a cape and a downwelling center at its upstream side which are effected in the SST as confirmed by the data and model results. The upwelling center leads to a density variation that causes an additional pressure gradient which advects the upwelling centers toward the northeast. This advection process induced by the density gradient cannot last for a long time if the upwelling process is stopped. However, if there is a longer period of southwesterly wind, the wind induced pressure gradient will support the advection processes which additionally causes the enlargement of the cold water center. The confirmation of these processes can explain the uneven distribution of upwelling centers and their temporal development as it is observed from satellite and observational data.

[46] **Acknowledgments.** We would like to thank our colleagues Bernhard Mayer and Hartmut Hein for model setup and discussion, Dagmar Hainbucher, Kieran O'Driscoll, and Anja Schneehorst for revising the paper, and Peter Damm for providing the NCEP data. This work was performed in the frame of the project "Land-Sea Interactions along Coastal Ecosystems of Tropical China: Hainan (LANCET)" under grant BMBF-03F0457B. We are grateful to two anonymous reviewers for their constructive comments, which improved our manuscript.

References

Backhaus, J. O. (1985), A three-dimensional model for the simulation of shelf sea dynamics, *Dtsch. Hydrogr. Z.*, *38*, 165–187.

Barron, C. N., and A. B. Kara (2006), Satellite-based daily ssts over the global ocean, *Geophys. Res. Lett.*, *33*, L15603, doi:10.1029/2006GL026356.

Capet, X. J., P. Marchesiello, and J. C. McWilliams (2004), Upwelling response to coastal wind profiles, *Geophys. Res. Lett.*, *31*, L13309, doi:10.1029/2004GL020123.

Chai, F., H. Xue, and M. Shi (2001), Upwelling east of Hainan Island, *Oceanogr. China*, *13*, 129–137.

Chapman, D. C., and D. B. Haidvogel (1992), Formation of Taylor caps over a tall isolated seamount in a stratified ocean, *Geophys. Astro. Fluid*, *64*(1), 31–65.

Chu, P. C., N. L. Edmons, and C. Fan (1999), Dynamical mechanisms for the South China Sea seasonal circulation and thermohaline variabilities, *J. Phys. Oceanogr.*, *29*(11), 2971–2989.

Davies, P. A. (2006), Experiments on Taylor columns in rotating stratified fluids, *J. Fluid Mech.*, *54*(4), 691–717.

Deng, S., and H. L. Zhong (1995), On relation between upwelling off Qionghai and fishery, *J. Oceanogr. Taiwan Strait*, *14*(1), 51–56.

Dippner, J. W., K. V. Nguyen, H. Hein, T. Ohde, and N. Loick (2007), Monsoon-induced upwelling off the vietnamese coast, *Ocean Dyn.*, *57*(1), 46–62.

Dong, C. M., and L. Y. Oey (2005), Sensitivity of coastal currents near point conception to forcing by three different winds: ECMWF, COAMPS, and blended SSM/I-ECMWF-buoy winds, *J. Phys. Oceanogr.*, *35*(7), 1229–1244.

Ekman, V. W. (1905), On the influence of the Earth's rotation on ocean currents, *Arch. Math. Astron. Phys.*, *2*(11), 1–52.

Enriquez, A. G., and C. A. Friehe (1995), Effects of wind stress and wind stress curl variability on coastal upwelling, *J. Phys. Oceanogr.*, *25*(7), 1651–1671.

Graham, W. M., and J. L. Largier (1997), Upwelling shadows as nearshore retention sites: The example of northern Monterey Bay, *Cont. Shelf Res.*, *17*(5), 509–532.

Guo, F., M. C. Shi, and Z. W. Xia (1998), Two-dimensional diagnose model to calculate upwelling on offshore of the east coast of hainan island, *Acta Oceanol. Sinica*, *20*(6), 109–116.

Hein, H. (2007), Vietnam upwelling—Analysis of the upwelling and related processes in the coastal area of south vietnam, Ph.D. thesis, Univ. of Hamburg, Hamburg, Germany.

Hsu, M. K., and A. K. Liu (2000), Nonlinear internal waves in the South China Sea, *Can. J. Remote Sens.*, *26*, 72–81.

Hu, J. Y., H. Kawamura, and D. L. Tang (2003), Tidal front around the Hainan Island, northwest of the South China Sea, *J. Geophys. Res.*, *108*(C12), 3342, doi:10.1029/2003JC001883.

Kalnay, E., et al. (1996), The NCEP/NCAR 40-year reanalysis project, *Bull. Am. Meteorol. Soc.*, *77*(3), 437–471, doi:10.1175/1520-0477(1996)077.

Kara, A. B., and C. N. Barron (2007), Fine-resolution satellite-based daily sea surface temperatures over the global ocean, *J. Geophys. Res.*, *112*, C05041, doi:10.1029/2006JC004021.

Killworth, P. (1978), Coastal upwelling and kelvin waves with small longshore topography, *J. Phys. Oceanogr.*, *8*(2), 188–205.

Kuo, N. J. (2000), Satellite observation of upwelling along the western coast of the South China Sea, *Remote Sens. Environ.*, *74*(3), 463–470, doi:10.1016/S0034-4257(00)00138-3.

Lee, H. J., S. Y. Chao, K. L. Fan, and T. Y. Kuo (1999), Tide-induced eddies and upwelling in a semi-enclosed basin: Nan Wan, *Estuarine Coastal Shelf Sci.*, *49*(6), 775–787, doi:10.1006/ecss.1999.0524.

Levitus, S., T. P. Boyer, and J. Antonov (1994), World ocean atlas 1994: vol. 5: Interannual variability of upper ocean thermal structure, *Tech. Rep. PB–95-270120/XAB*, National Environmental Satellite, Data, and Information Service, Washington, D. C.

MacCready, P., and P. B. Rhines (1993), Slippery bottom boundary layers on a slope, *J. Phys. Oceanogr.*, *23*(1), 5–22, doi:10.1175/1520-0485(1993)023.

Narimousa, S., and T. Maxworthy (1986), Coastal upwelling on a sloping bottom: The formation of plumes, jets and pinched-off cyclones, *J. Fluid Mech.*, *176*, 169–190.

Oke, P. R., and J. H. Middleton (2000), Topographically induced upwelling off eastern australia, *J. Phys. Oceanogr.*, *30*(3), 512–531, doi:10.1175/1520-0485(2000)030.

Orr, M. H., and P. C. Mignerey (2003), Nonlinear internal waves in the South China Sea: Observation of the conversion of depression internal waves to elevation internal waves, *J. Geophys. Res.*, *108*(C3), 3064, doi:10.1029/2001JC001163.

Pickett, M. H., and J. D. Paduan (2003), Ekman transport and pumping in the California Current based on the US Navy's high-resolution atmospheric model (COAMPS), *J. Geophys. Res.*, *108*(C10), 3327, doi:10.1029/2003JC001902.

Pohlmann, T. (1987), A three dimensional circulation model of the South China Sea, in *Three Dimensional Models of Marine and Estuarine Dynamics*, edited by J. N. B. Jamart, pp. 245–268, Elsevier, Amsterdam.

Pohlmann, T. (1996a), Calculating the development of the thermal vertical stratification in the north sea with a three-dimensional baroclinic circulation model, *Cont. Shelf Res.*, *16*(2), 163–194.

Pohlmann, T. (1996b), Predicting the thermocline in a circulation model of the North Sea. Part 1. Model description, calibration and verification, *Cont. Shelf Res.*, *16*(2), 131–146.

Pohlmann, T. (2006), A meso-scale model of the central and southern North Sea: Consequences of an improved resolution, *Cont. Shelf Res.*, *26*(19), 2367–2385, doi:10.1016/j.csr.2006.06.011.

Rosenfeld, L. K., F. B. Schwing, N. Garfield, and D. E. Tracy (1994), Bifurcated flow from an upwelling center: a cold water source for Monterey Bay, *Cont. Shelf Res.*, *14*(9), 931–964.

Shaw, P. T., and S. Y. Chao (1994), Surface circulation in the South China Sea, *Deep Sea Res. I*, *41*(11–12), 1663–1683.

Song, Y. T., and Y. Chao (2004), A theoretical study of topographic effects on coastal upwelling and cross-shore exchange, *Ocean Modell.*, *6*(2), 151–176.

Song, Y. T., D. B. Haidvogel, and S. M. Glenn (2001), Effects of topographic variability on the formation of upwelling centers off New Jersey: A theoretical model, *J. Geophys. Res.*, *106*(C5), 9223–9240.

Su, J. L. (2004), Overview of the South China Sea circulation and its influence on the coastal physical oceanography outside the Pearl River Estuary, *Cont. Shelf Res.*, *24*(16), 1745–1760, doi:10.1016/j.csr.2004.06.005.

Wang, Y. G., G. H. Fang, Z. X. Wei, F. L. Qiao, and H. Y. Chen (2006), Interannual variation of the South China Sea circulation and its relation to El Nino, as seen from a variable grid global ocean model, *J. Geophys. Res.*, *111*, C11S14, doi:10.1029/2005JC003269.

Weisberg, R. H., Z. Li, and F. Muller-Karger (2001), West Florida shelf response to local wind forcing—April 1998, *J. Geophys. Res.*, *106*(C12), 31,239–31,262.

Xie, S. P., Q. Xie, D. X. Wang, and W. T. Liu (2003), Summer upwelling in the South China Sea and its role in regional climate variations, *J. Geophys. Res.*, *108*(C8), 3261, doi:10.1029/2003JC001867.

Yang, J., and J. F. Price (2000), Water-mass formation and potential vorticity balance in an abyssal ocean circulation, *J. Mar. Res.*, *58*(5), 789–808.

T. Pohlmann and J. Su, Institute of Oceanography, Centre for Marine and Climate Research, University of Hamburg, Bundesstrasse 53, D-20146 Hamburg, Germany. (jian.su@zmaw.de; pohlmann@ifm.uni-hamburg.de)